

Theoretical strength and prediction of structural defects in metallic glassesZhukun Zhou,^{1,3} Hao Wang,^{2,*} and Mo Li^{1,3,†}¹*State Key Laboratory of Powder Metallurgy, Central South University, Changsha 410032, China*²*Guangdong Provincial Key Laboratory of Micro/Nano Optomechatronics Engineering, College of Mechatronics and Control Engineering, Shenzhen University, Shenzhen, 518060, China*³*School of Materials Science and Engineering, Georgia Institute of Technology, Atlanta, Georgia 30332, USA*

(Received 15 February 2019; revised manuscript received 4 June 2019; published 24 July 2019)

Theoretical strength plays a pivotal role in gauging the maximum stress and inferring structural defects in crystalline materials. However, its very existence and the expected prediction of possible defects in amorphous solids remain elusive. Here, by using a finite deformation theory, we obtain the theoretical strengths for several bulk metallic glasses under pure shear loading. The theoretical strengths obtained are only several times larger than the experimental yield stresses; in contrast, they are three or four orders of magnitude higher in crystalline materials. This striking closeness between the theoretical and experimental strengths suggests the absence of any extended structural defects that can substantially reduce the intrinsic strength in the amorphous metals. Instead, the atoms have to sever each individual bond to deform. Further investigation reveals that the deformation occurring at the theoretical stress proceeds with the mechanical instability with a vanishing shear modulus, or a mechanical spinodal. We deduce from these results that, different fundamentally from crystalline solids, there are no extended structural defects in the amorphous solids and the plastic deformation must be local and sensitive to sample conditions.

DOI: [10.1103/PhysRevB.100.024109](https://doi.org/10.1103/PhysRevB.100.024109)**I. INTRODUCTION**

Theoretical strength refers to the maximum stress that a material can withstand. For crystalline materials, the maximum strength is achieved when they do not contain extended structural defects [1–5]. Traditionally, there are two ways to obtain the theoretical strength. One is from the mean-field theory such as the Frenkel model [1] and the other by using the nonlinear elasticity theory [5]. *Ab initio* quantum calculation is a modern approach [6–9] which relies on numerical modeling rather than the analytical theories. Experimentally, the maximum strength comes only from those materials without or with less detrimental crystal defects or imperfections, such as crystal whiskers [10]. The theoretical strength predicted from Frenkel’s model is three or four orders of magnitude higher than the observed values measured in real crystalline materials in the experiments. Nevertheless, it was the revelation of the existence of the theoretical strength that ignited the search and discovery of the crystal defect, i.e., dislocations [11,12]: In order to reconcile the huge difference between the theoretical and experimental yield strength the concept of dislocation, an extended crystal structural defect, was introduced.

In amorphous solids, the concept of theoretical strength and the familiar routine of predicting structural defects from the theoretical strength face many fundamental challenges. Firstly, amorphous solids are topologically disordered down to atomic scales. Therefore, defining a structural “defect” in

an amorphous solid becomes conceptually difficult. Secondly, without the long-range order like in crystalline materials, it is technically impossible to set up an analytical theory like the Frenkel model that is premised on the translational crystalline symmetry [1]. Thirdly, the modern quantum computation, which has enjoyed a great success in crystalline materials because of their translational symmetry, will run into many difficulties in modeling amorphous solids, one of which is the size effect. Without the translational symmetry, one is required to have a large enough sample to produce statistically reliable results such as the theoretical strength. However, current computing capability limits the number of atoms to a few hundred atoms, which is far fewer than that required to be free of the size effect [13]. Due to these reasons, there is little progress in the exploration of the theoretical strength in amorphous solids. Consequently, the expected prediction of the structural defects has not been carried out.

In this work, we use a finite deformation theory to obtain the desired theoretical strengths for several bulk metallic glasses under pure shear loading. The chief result is that the theoretical strengths obtained analytically are only several times higher than the experimentally measured yield or fracture stresses (see Table I). Note that, in general, yielding and fracture in the amorphous solids occur at the same point in experiments. This striking closeness between the theoretical and experimental strength strongly suggests the absence of any extended structural defects that could substantially reduce the intrinsic strength in the amorphous metals. Further investigation reveals that yielding occurring at the theoretical strength proceeds with the mechanical instability with a vanishing mechanical response function represented by the shear modulus. In other words, failure in metallic glasses

*whao@szu.edu.cn

†mo.li@mse.gatech.edu

TABLE I. The theoretical Strengths (τ_{\max}) and the corresponding shear strains (η_{\max}) of the three bulk metallic glasses from the finite deformation theory. $\tau_{0.2\%}$ is the yield stress evaluated using the 0.2% offset strain method in order to compare with the experimentally measured yield stress. G_0 is the shear modulus in the undeformed state.

	Relaxed (GPa)		Unrelaxed (GPa)		0.2% Offset strain (GPa)	Experiment (GPa)	Relaxed
	τ_{\max}	η_{\max}	τ_{\max}	η_{\max}	$\tau_{0.2\%}$	τ	
Theoretical strength and strain							
Zr _{52.5} Ti ₅ Cu _{17.9} Ni _{14.6} Al ₁₀	4.79 ^a	0.11 ^a	5.22 ^a	0.12 ^a	1.25	2.5–3.5 ^b	0.152 ^a
	5.24 ^c	0.11 ^c	7.01 ^c	0.16 ^c		1.016 ^d , 0.842 ^e	0.166 ^c
Pd ₄₀ Cu ₃₀ Ni ₁₀ P ₂₀	3.40 ^a	0.07 ^a	4.60 ^a	0.1 ^a	1.41	0.82 ^d	0.095 ^a
	3.82 ^c	0.08 ^c	6.02 ^c	0.12 ^c		1.41–1.85 ^b	0.107 ^c
Zr _{41.2} Ti _{13.8} Cu _{12.5} Ni ₁₀ Be _{22.5}	6.09 ^c	0.11 ^c	8.74 ^c	0.17 ^c	1.52	3.1 ^b , 0.95 ^d	0.160 ^c

^aFrom the current theory with up to the fourth-order terms of the strains included.

^bThe maximum shear stresses from the nanoindentation [25,26,29].

^cFrom the current theory with the third-order terms of the strains included.

^dThe maximum shear stresses estimated from a tensile tests [27,30,31].

^eThe maximum shear stresses estimated from a shear deformation [28].

at the maximum stress resembles a mechanical “spinodal” transition: At the failure point, the atomic displacement or deformation becomes an unstable event. Any local deformation initiated can spread out with little resistance to forming larger deformation zones. We argue that due to this particular mechanism, the deformation and failure of metallic glasses must be local and sensitive to sample conditions, which is fundamentally different from crystalline materials.

II. THEORY

To obtain the maximum stress, the theoretical stress-strain relation needs to be obtained analytically. In the finite deformation theory, this relationship is furnished by a series expansion of the free energy F of the system under deformation beyond the second-order strain terms (see Appendix A) [14]. Since metallic glasses are known experimentally to have large elastic strain limits in the range of 2%–3%, the expansion to the third or fourth order is necessary and naturally justified.

Specifically, to obtain the shear stress as a function of the applied shear strain we subject metallic glass samples to a pure shear deformation with the strain tensor

$$\begin{pmatrix} \eta_{11} & \eta_{12} & 0 \\ \eta_{21} & \eta_{22} & 0 \\ 0 & 0 & \eta_{33} \end{pmatrix},$$

where $\eta_{12} = \eta_{21} = \eta$ is the applied shear strain on a shear plane and η_{11} , η_{22} , and η_{33} are the normal strains along the x , y , and z (or 1, 2, and 3) directions. *The normal strains are induced by the applied shear strain.* Here, the normal strains are obtained when we allow the shear-induced normal stresses going to zero, or relaxed out (see Appendix B). Under these conditions, the shear stress can be obtained analytically as a function of the shear strain, as well as the induced normal strains; that is, $\sigma_{12} = f(\eta)|_{\eta_{11}, \eta_{22}, \eta_{33}}$. The explicit expression for the stress-strain relation is given in Eq. (A3) in Appendix A. The procedure of acquiring σ_{12} is given in Appendix B. Therefore, the theoretical strength can be obtained from the shear stress-strain curve at the point of the maximum stress.

To extract the underlying mechanisms of the deformation at the theoretical stress, we need another mechanical quantity, the elastic constant matrix C , which is the Hessian or the second-order derivatives of the free energy F with respect to the deformation strains (see Appendix C). C is related to the mechanical response function of the system to the applied deformation strain, which is defined by the tensor $B_{ijkl} = \partial\sigma_{ij}/\partial\eta_{kl} + O(\eta)$. The response function B is similar to the familiar magnetic susceptibility for magnetic materials under applied magnetic field [15,16]. Under large deformation, the elastic response function B becomes strain dependent. Its magnitude and trend of variation with the applied stress or strain tell us not only how “strong” a material is when deformed but also the mode of deformation, i.e., the eigenstrains, as well as the possible defects either pre-existing or caused by the external applied loading. For these reasons, B is called the elastic stiffness coefficient, which is related to the elastic constant C'_{ijkl} in the deformed state [see Eqs. (D1) in Appendix D] and applied stress τ_{ij} , $B_{ijkl} = C'_{ijkl} + (\delta_{ik}\tau_{jl} + \delta_{jk}\tau_{il} + \delta_{il}\tau_{jk} + \delta_{jl}\tau_{ik} - 2\delta_{kl}\tau_{ij})/2$ [15–17], where δ_{ij} is the Kronecker delta function. Here, the Einstein summation convention is used.

Under an applied strain or stress, the elastic stiffness coefficient B behaves in two different ways. One is that it decreases but remains finite below and at the maximum stress, and the other is that it approaches zero at the maximum stress. In the former, the system is said to be stable up to the maximum stress, although weakened mechanically; and the latter indicates that the system experiences a *mechanical instability*. In other words, at the instability point, with a small increment of applied strain or stress, the system becomes thermomechanically unstable with the development of a large, unbounded deformation strain in its mechanical response. This scenario corresponds to either failure or shear band formation, which are the two natural consequences of the instability in deformation of metallic glasses.

For a tensor quantity like B , the instability versus the applied deformation strain is represented by the condition $|\bar{B}_{ijkl}| \rightarrow 0$ (see Appendix D), where $\bar{B} = (B^T + B)/2$ is the symmetrized tensor B . Similar to the chemical spinodal,

TABLE II. The experiment data of the second-, third-, and fourth-order elastic constants in the undeformed state of the metallic glasses measured using ultrasound [18–20].

	Zr _{52.5} Ti ₅ Cu _{17.9} Ni _{14.6} Al ₁₀ (GPa)	Pd ₄₀ Cu ₃₀ Ni ₁₀ P ₂₀ (GPa)	Zr _{41.2} Ti _{13.8} Cu _{12.5} Ni _{10.0} Be _{22.5} (GPa)
c_{11}	155.7	216.9	164.68
c_{12}	92.7	145.3	88.34
c_{44}	31.5	35.8	38.17
c_{111}	-1230.2	-2285.4	-1414.5
c_{112}	-389.4	-695	-445.3
c_{123}	-109	-227	-185.1
c_{144}	-140.2	-234	-130.1
c_{155}	-210.2	-397.6	-242.3
c_{456}	-35	-81.8	-56.1
c_{1111}	6926.9	-4062.7	
c_{1112}	1236.2	-1830	
c_{1122}	-1869.7	-3218.2	
c_{1123}	-582.6	-1026	
c_{1144}	-643.55	-1096.1	
c_{1155}	948.4	-372.1	
c_{1255}	454.7	-201	
c_{1266}	1250.7	161	
c_{1456}	398	181	
c_{4444}	-453.4	-799.7	
c_{4455}	-151.1	-266.6	

we call this instability the “mechanical spinodal.” For a stable system, the matrix of the elastic stiffness coefficient should remain positive definite, or the free energy hypersurface should remain convex versus the strains [15,16]. The instability condition, on the other hand, represents the concaveness in the free energy hypersurface, which characterized by six separate criteria, each of which corresponds to a possible bifurcation of the system along a specific deformation path [16] in the six-dimensional strain space [see Eqs. (D2a)–(D2f) in Appendix D]. From the deformation mode and strain that correspond to the first occurrence of the instability condition approached in the system under shear, we can identify the underlying deformation mechanism and whether this mechanism is intrinsic to the failure corresponding to the maximum stress.

Note that the finite deformation theory applies to the elastic regime, albeit at large nonlinear strains. The prediction of the defect process and the defects-related large deformation, including plasticity, is beyond the scope of this work. We can, however, predict the mechanical responses at the elastic limit represented by the maximum stress and the instability. In metallic glasses, the plastic deformation involving shear band formation needs a separate treatment in addition to the nonlinear elastic theory. Fortunately, our theory may even be more relevant in practice since most metallic glasses fail or yield at the end of an elastic limit.

III. METHODS

As shown in Appendixes A and B, in order to obtain the stress-strain relations [Eq. (A1)], the elastic stiffness coefficients [Eqs. (C1a)–(C1j)] and the instability conditions [Eqs. (D2a)–(D2f)], the finite deformation theory needs

to be implemented with the input of the corresponding second-, third-, and fourth-order elastic constants measured from experiments. These elastic constants are measured using ultrasound. For the second-order elastic constants, the measurement is done in the undeformed state, i.e., when there is no external shear strain or stress applied. For the higher-order elastic constants, external deformation strains need to be applied to the sample while the ultrasound is transmitted in the sample. Various forms of deformation strains have to be applied to the sample in order to obtain the higher-order elastic constants. Under the prefixed deformations, these elastic constants are measured from the sound velocities. So far, these data are available for only a few bulk metallic glasses, Zr_{52.5}Ti₅Cu_{17.9}Ni_{14.6}Al₁₀(Vit105) [18], Pd₄₀Cu₃₀Ni₁₀P₂₀ [19], and Zr_{41.2}Ti_{13.8}Cu_{12.5}Ni_{10.0}Be_{22.5}(Vit1) [20], although only up to the third-order elastic constants are available for Vit1. The input elastic constants used in our theory are listed in Table II and the procedure to implement the theory using these constants is described in Appendix E.

Note that the elastic constants measured using ultrasound are adiabatic, while the input elastic constants needed in the finite deformation theory are isothermal. However, their difference is small at room temperature. For example, for Vit105, $C_{11}^S - C_{11}^T = C_{12}^S - C_{12}^T = B_S - B_T = \frac{TV\beta}{C_V} B_T^2 = \frac{TV\beta}{C_P} B_T B_S$, where T is temperature; V is volume; β is the thermal expansion coefficient; C_P and C_V are the heat capacity at constant pressure P and volume V , respectively; and B_S and B_T are the adiabatic and isothermal bulk modulus. Here, for all quantities the superscript or subscript S stands for the adiabatic and T for the isothermal condition. For Vit 105, at 300 K the thermal expansion coefficient is 10^{-5} K^{-1} [21], the specific heat capacity at constant pressure is $1177 \text{ J g atom}^{-1} \text{ K}^{-1}$ [22], and the adiabatic bulk modulus B_S is 113.7 GPa [18].

Hence, the difference between the adiabatic and isothermal elastic constant $C_{11}^S - C_{11}^T$ in metallic glass Vit105 is only about 0.33 GPa. Therefore, we can ignore the difference and instead use the experimentally measured adiabatic elastic constants in our theory.

IV. RESULTS AND DISCUSSIONS

A. Theoretical stresses

Figure 1 shows the shear stress-strain relations obtained analytically for the three bulk metallic glasses. For $Zr_{52.5}Ti_5Cu_{17.9}Ni_{14.6}Al_{10}$ and $Pd_{40}Cu_{30}Ni_{10}P_{20}$, the fourth-order shear strain terms are included, while only up to the third-order terms for $Zr_{41.2}Ti_{13.8}Cu_{12.5}Ni_{10}Be_{22.5}$ are available. As shown, the shear stress-strain relations exhibit a linear elastic regime in the small strain region. The theory is also able to predict a larger nonlinear elastic regime. Since the yielding occurs at a yielding stress with a large, nonlinear strain, we need to determine the yield point by using the conventional 0.2% strain offset method (Table I). This is done by drawing a linear stress-strain line that has the shear modulus determined near zero shear strain but with an offset shift of 0.2% shear strain at zero stress. The interception of the line with the stress-strain curve in Fig. 1 gives the yield point. Beyond the yield point, the shear stress continues to rise (nonlinearly) until it hits a maximum stress.

Note that different from the common observations in experiments, the samples do not fail or fracture at the yielding point nor at the maximum stress in the theory. This is because we used the samples in the theory without any boundaries. A boundaryless sample would continuously deform under shear. Another reason is that the samples in the theoretical models do not contain imperfections or surface cracks that can cause premature failure initiated from these sites that leads to the discontinuity in the stress-strain relation.

To illustrate the importance of relaxation of the shear-induced internal normal stresses, in Fig. 1 we show the shear-induced normal stresses when the samples are not allowed to get rid of them by relaxation. One can see that the shear-induced normal stresses are compressive in nature and their magnitudes are comparable to the shear stress. Unlike the shear stress that reaches a maximum and then decreases, the compressive normal stresses keep rising with the shear strain. In this case, therefore, the samples are affected effectively by the increasing compression from the normal stresses in addition to the applied shear. Therefore, the emergence of strong shear-normal stress coupling is expected. As shown below, the unique influence of the induced normal stress on shear in the amorphous solids is demonstrated when we relax these internal stresses.

Upon relaxation, which allows the samples to change sizes along the normal stress directions, the normal stresses go to zero. As a result, the normal strains are generated and the shear stress-strain relation curve becomes less steep, although for Vit105 the effect is smaller than the others. The relaxation corresponds to the experimental condition where the induced normal stresses are naturally relaxed during the designated loading, such as shear stresses, if the samples are not confined on the boundary. From the relaxed stress-strain relations, we

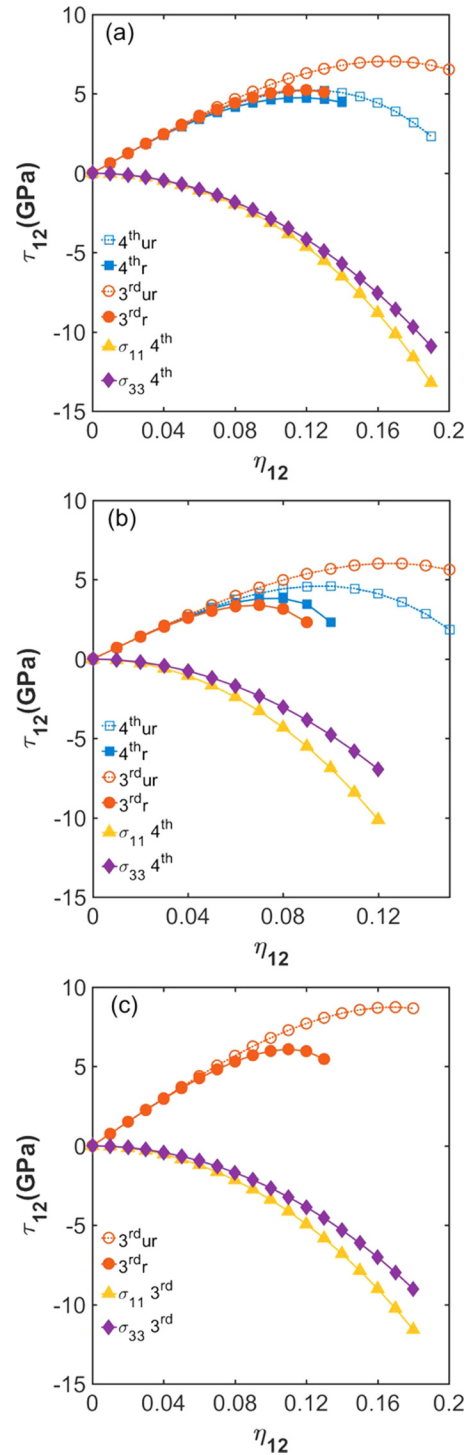


FIG. 1. The shear stress-strain relations and the induced normal stresses for (a) $Zr_{52.5}Ti_5Cu_{17.9}Ni_{14.6}Al_{10}$ (Vit105), (b) $Pd_{40}Cu_{30}Ni_{10}P_{20}$, and (c) $Zr_{41.2}Ti_{13.8}Cu_{12.5}Ni_{10.0}Be_{22.5}$ (Vit1) under pure shear loading from the finite deformation theory. Note that for Vit1, the theory has only up to the third-order terms in the shear strain since the fourth-order elastic constants are not available. Legend: “4u” denotes “the fourth-order theory with the normal stresses unrelaxed”, “4r” “the fourth-order theory with the normal stresses relaxed, and so on. The corresponding shear-induced normal stresses, σ_{11} , σ_{22} ($= \sigma_{11}$), and σ_{33} , are calculated from the fourth-order theory without stress relaxation in (a) and (b) and from the third-order theory in (c).

can obtain the theoretical shear strength by locating the maximum stress value on the curve and the corresponding strain. The results are tabulated in Table I. To show the influence of the internal normal stresses, we also give the maximum shear stresses without relaxation of the internal normal stresses.

For glasses $\text{Zr}_{52.5}\text{Ti}_5\text{Cu}_{17.9}\text{Ni}_{14.6}\text{Al}_{10}$ and $\text{Pd}_{40}\text{Cu}_{30}\text{Ni}_{10}\text{P}_{20}$ with the fourth-order terms considered, the critical shear strengths are 4.79 and 3.40 GPa at the corresponding shear strain of 0.11 and 0.07, respectively, with the shear-induced normal stresses relaxed. Without relaxation, the strengths are higher, namely, 5.22 and 4.60 GPa at the corresponding strains of 0.12 and 0.1 which are also larger. For $\text{Zr}_{41.2}\text{Ti}_{13.8}\text{Cu}_{12.5}\text{Ni}_{10.0}\text{Be}_{22.5}$, since only up to the third-order terms are included, the theoretical strength with relaxed and unrelaxed normal stresses are much higher than the other two systems, at 6.09 and 8.74 GPa with the corresponding maximum strain at 0.11 and 0.17, respectively. It appears that the inclusion of the fourth-order terms can also lead to “relaxation,” or a softening effect.

To further test the effect of the fourth-order terms, we deliberately omitted the fourth-order terms in $\text{Zr}_{52.5}\text{Ti}_5\text{Cu}_{17.9}\text{Ni}_{14.6}\text{Al}_{10}$ and $\text{Pd}_{40}\text{Cu}_{30}\text{Ni}_{10}\text{P}_{20}$ which have both third- and fourth-order terms. The results are given in Fig. 1 and Table I. These results indicate that, indeed, both the relaxation of the normal stress and the inclusion of the fourth-order terms of the shear strains have a similar and significant impact on the maximum stress and strain: The relaxation and the inclusion of the fourth-order terms lower both the stress and strain. Note that traditionally, however, only the third-order terms are considered in nonlinear theories to introduce the so-called “anharmonic” correction to the linear description of deformation [23,24]. Our work shows that the higher-order terms are important, which act effectively as a relaxation to the stress and strain from the lower-order theory. Therefore, higher-order terms are necessary for obtaining reliable results, including the theoretical strengths.

B. Mechanical instability conditions and deformation mode at the maximum stress

Next, we take a look at the instability conditions via the elastic stiffness coefficients versus the applied shear strain in the three bulk metallic glasses. We found that all six stability criteria [Eqs. (D2a)–(D2f) in Appendix D], i.e., the condition for $|\bar{B}_{ijkl}|$, remain positive definitive (Fig. 2). They show the decreasing trends as the shear deformation strain increases, and all except the criterion in Eq. (D2f) remain positive before and at the maximum stress. In other words, the instability, which occurs when the stability criterion becomes zero, does happen at the maximum shear strain. When the shear stability criterion described in Eq. (D2f) is violated, or approaches zero while other conditions are not, the material fails via a *shear instability*.

Figure 2 shows a large decline in the shear stability criterion described in Eq. (D2f) as the shear strain increases, and the shear stability criterion reaches zero at exactly the corresponding state of the maximum shear strain and stress. Further analysis shows that the criterion in Eq. (D2f) is directly related to the shear modulus of

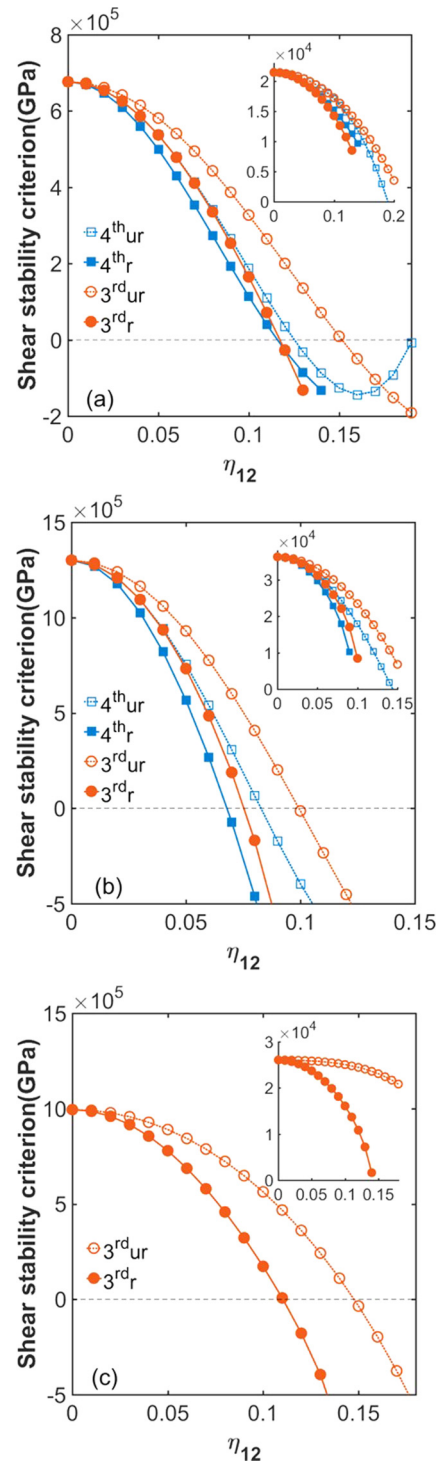


FIG. 2. The elastic stiffness coefficients in Eq. (D2f) versus applied shear strain for (a) $\text{Zr}_{52.5}\text{Ti}_5\text{Cu}_{17.9}\text{Ni}_{14.6}\text{Al}_{10}$ (Vit105), (b) $\text{Pd}_{40}\text{Cu}_{30}\text{Ni}_{10}\text{P}_{20}$, and (c) $\text{Zr}_{41.2}\text{Ti}_{13.8}\text{Cu}_{12.5}\text{Ni}_{10.0}\text{Be}_{22.5}$ (Vit1) under pure shear loading from the finite deformation theory. Note that for Vit1, the theory has only up to the third-order shear strain since the fourth-order elastic constants are not available. The insets in each figure are the stability condition in Eq. (D2c), or the denominator in the shear modulus G . For comparison, we also include the results from the finite deformation theory with up to the third-order terms. Legend: “4u” denotes “the fourth-order theory with the normal stresses unrelaxed,” “4r” “the fourth-order theory with the normal stresses relaxed,” and so on.

the bulk metallic glasses under pure shear. Under the deformation, the shear modulus depends on the deformation strains and its analytical expression can be obtained as
$$G = - \frac{(\bar{B}_{11} + \bar{B}_{12})(\bar{B}_{36}^2 - \bar{B}_{33}\bar{B}_{66}) + 2\bar{B}_{16}(\bar{B}_{16}\bar{B}_{33} - \bar{B}_{13}\bar{B}_{36}) + 2\bar{B}_{13}(\bar{B}_{13}\bar{B}_{66} - \bar{B}_{16}\bar{B}_{36})}{(\bar{B}_{11} + \bar{B}_{12})\bar{B}_{33} - 2\bar{B}_{13}^2},$$
 where the numerator is the shear stability criterion in Eq. (D2f) and the denominator is that in Eq. (D2c). As shown in the insets in Fig. 2, the condition in the denominator remains finite and positive before and at the maximum stress. Therefore, at the maximum strain and stress, all three bulk metallic glasses become unstable with the vanishing of the shear modulus; i.e., they experience a shear instability. In other words, when the system reaches the maximum stress, the failure deformation mode is shear.

The zero shear modulus at this point indicates vanishing resistance to shear at the maximum stress. In other words, the simultaneous vanishing of the shear modulus and the elastic stiffness coefficient B at the maximum stress indicates that the system can develop a large shear strain under a small stress variation or perturbation, and the shear deformation becomes unbounded or without resistance. This property resembles a spinodal transition, albeit mechanical in nature. We can reasonably believe that this mechanism may lie behind the yielding and plastic deformation involving shear band formation, although a precise description requires a separate theoretical treatment.

C. Absence of extended structural defects, or presence of the strong tendency of local mechanical deformation

Metallic glass is often regarded as strong with the shear stress “approaching the theoretical strength” [32]. However, little is known about the exact value of the theoretical strength. Our theory gives an estimate of the theoretical shear strength in bulk metallic glasses [33]. We found that the fully relaxed samples with no shear-induced internal normal stresses present have their theoretical shear strength values are only higher by less than an order of magnitude than the experimentally known maximum values, i.e., yield or fracture stresses (see Table I). This closeness between the theoretical and experimental strengths is striking as compared with the crystalline materials where one often finds three to four orders of magnitude difference [34]. Such a large difference prompted the search for new deformation mechanisms in real crystalline materials that would lower the theoretical strength. One of these proposals is the dislocation [35–37]. Dislocations are an extended structural defect with the faulty atomic arrangement out of the perfect crystal order. It was confirmed later that the motion of the dislocation fault lines on the atomic planes causes yielding that requires much lower shear stress [38,39]. Therefore, it is concluded that the existence of the dislocations is the origin of the much lower strength in real crystals.

However, the amorphous structure, such as metallic glasses, is already heavily defected down to the atomic scales. In other words, no two atoms have the same local atomic packing environment. Such a disordered structure makes it impossible to have any well-organized, extended structural defects. Therefore, it is conceptually difficult to imagine any atomic movement on the extended length scale involving a large group of atoms in any “fault lines” such as dislocations, or any other type of well-defined correlated motion of a

large number of atoms under shear stress. Instead, *atoms have to move individually according to the allowance of their own environments*. The outcome of this scenario is that atoms have to move individually at the yielding point by severing their atomic bonds with the rest of the atoms. This action of “cutting” the individual atomic bonds, incidentally, is the original proposal of the atomic mechanism of yielding in perfect crystals [40]. In crystals, this mechanism leads to extraordinarily high stresses, the theoretical strengths. In this work, the closeness of the theoretical strength to the experimental yield stress in metallic glasses suggests that this “individual atom motion” is the mechanism. In other words, this mechanism, rejected by the early works in crystalline materials, may hold true in metallic glasses as each atom has to move individually by executing shear deformation relative to other atoms in each atom’s individual environment. This unique deformation mechanism in the amorphous structure is the reason why the experimental strength is so high and close to the theoretical one.

Following the argument, we may deduce that there is no extended structure defect that can substantially reduce the theoretical strength in real metallic glasses. In this case, metallic glasses must have a strong tendency to deform locally whenever the local environment permits. This conclusion leads us to several interesting explanations for the mechanical behaviors in real metallic glasses:

Since the difference between the theoretical and actual strength is small, it is very easy for a real metallic glass to reach the theoretical strength, albeit in local regions. This can be achieved via various stress concentrators such as sample imperfections and other heterogeneities present in real glassy materials. These imperfections and heterogeneities may function as the predominant deformation initiators and carriers: Once the local deformation starts from these places where the theoretical strength is reached, it spreads out to the rest of the sample. As shown above, since the local deformation is driven by the local stress, the rate of deformation is dominated by the stress level there: Whenever the theoretical stress is approached, deformation occurs and grows. Unlike dislocations in crystalline materials, these stress fields are local and easy to change or adapt to the local environment. Thus, they do not show strong interactions as the dislocations in crystalline materials. This may well be the origin for the lack of work hardening in metallic glasses at the yielding or the maximum stress point.

This particular aspect of amorphous solids discussed above lends support to our use of the finite deformation theory to obtain the theoretical strength. In this theory, the only input is the experimentally measured elastic constants. These constants are measured from the acoustic sound waves in the metallic glasses. When the samples are not subject to any external deformation strain, one obtains the second-order elastic constants; when subject to the external strains, the acoustic wave velocity gives the higher-order elastic constants. In both cases, since the sound wavelength is far larger than the sizes of any perceivable imperfections such as surface crack or voids, the elastic constants measured are not significantly affected by them. Thus, the theoretical strength obtained using these constants is as if from the “imperfection-free,” or ideal samples.

On the other hand, since the samples are subject to certain deformation strains during the measurement of the higher-order elastic constants, any microscopic and nanoscale changes induced by the deformation, such as the “shear deformation zones” or “free volume” changes are present. Although the external applied deformation strains do not reach the yield point, these small and local deformations already occur under the external loading. These small deformation zones are statistically factored in the measured elastic constants. Therefore, the maximum stress obtained by the finite deformation theory using these elastic constants also reflects these internal structural changes intrinsic to the amorphous materials.

D. Mechanical spinodal and related deformation mechanisms

The above-proposed deformation mechanism with each atom deforming or cutting its bonds with other atoms individually at the maximum stress results in a rapid buildup of internal free energy. If no other stress relief mechanism exists, such as the dislocation in crystals, the individual atomic deformation would drive the system to the instability point where the free energy hypersurface loses its convexity. This corresponds to the instability conditions $|\bar{B}_{ijkl}| \rightarrow 0$ along the shear path. Since B_{ijkl} is the second-order derivative of the free energy with respect to the shear strain, the instability indicates a mechanical spinodal transition, which is like a continuous phase transition except without reversibility in our mechanically deformed samples. We should mention once again that this prediction is limited to the elastic regime or at the limit of the elastic regime. The large deformation behaviors in the plastic regime require different treatments.

In addition, we should mention that the metallic glasses in the finite deformation theory are treated as homogeneous; i.e., no other stress concentrators or heterogeneities and surfaces are present. In this sense, our model actually deals with a piece of amorphous solid that has no macroscopic or mesoscopic scale inhomogeneities with a size larger than the wavelength of sound. As mentioned in the previous sections, however, the effects from the smaller scale structural variation on the nanometers are already factored in, in part, in the theory via the measured second- and higher-order elastic constants, which is equivalent to a mean-field model. Therefore, although our sample is “homogeneous” and deformation is “uniform,” the theory is able to predict that the deformation in the sample occurs with the mechanism of “individual atomic shear” when the elastic instability is reached at the maximum strain. In pure shear, we show that the metallic glasses become mechanically unstable at the maximum stress via the shear instability. That is, the free energy hypersurface becomes buckled and changes from convex to concave along the deformation path of the shear strain. Further consideration of the inhomogeneous nature of the deformation in metallic glasses requires us to develop a new theory. The local deformations should be included explicitly, including the embryos and the fully grown shear bands. This can be done, for example, with the treatment in the Ginzburg-Landau type of theory [41].

In reality, the mechanical spinodal transition at the maximum strength depicted by the finite deformation theory may occur in local regions. Among many factors that interfere and disrupt the deformation path are the presence of microcracks, surface imperfections, voids from casting and processing, and other structural and chemical concentration heterogeneities. These “imperfections” are not extended structural defects but can act as the stress concentrators and promoters for local deformation. Due to the strong tendency of local deformation in amorphous solids, once the local stress reaches the critical stress in these regions, deformation occurs there. In other words, yielding occurs when the local instability condition is violated. This mechanism allows us also to explain why the strength of real metallic glasses is so close to the theoretical value.

V. CONCLUSIONS

The long-sought-after theoretical strength of metallic glasses is obtained by using a finite deformation theory. By including the higher-order terms of the deformation strains in the free energy, we are able to describe the stress-strain relation and the maximum stress that occurs at large deformation strains. The result shows that the theoretical strength is only a few times larger than the experimental failure stress. The small difference is dwarfed by the vast difference between the theoretical and experimental strengths on the order of three to four orders of magnitude in crystalline materials. This striking closeness between the two in amorphous metals suggests the absence of any extended structural defects that can substantially reduce the intrinsic strength difference.

In addition, we found that deformation at the theoretical strength proceeds with the mechanical instability, i.e., the vanishing mechanical response function and a mechanical spinodal transition. This phenomenon resembles that in the second-order phase transitions where the curvature of the free energy hypersurface becomes concave and the mechanical deformation becomes a runaway process. In light of the above results, we argue that the deformation mechanism in the disordered materials differs fundamentally from that in crystals; that is, failure in amorphous solids should proceed individually in each atom by severing its bonds with the rest of the atoms, and thus the deformation must be local and sensitive to sample conditions.

ACKNOWLEDGMENTS

M.L. would like to acknowledge the financial support from the National Thousands Talents Program of China and the Central South University. The support provided by China Scholarship Council (CSC) during a visit of Zhukun Zhou (201606370100) to Georgia Institute of Technology is acknowledged. This work was supported by National Natural Science Foundation of China (Grant No. 51771123), and the Shenzhen Peacock Innovation Project (Grant No. KQJSCX20170327151307811)

APPENDIX A

In the framework of the finite deformation theory, the stress in any state x from the state X in a solid under deformation can be expressed as [14]

$$\begin{aligned}\sigma_{ij}(x) &= \frac{1}{V(x)} \frac{\partial F(x)}{\partial \zeta_{ij}} \Big|_x = \frac{V(X)}{V(x)} \frac{\partial \eta_{kl}}{\partial \zeta_{ij}} \frac{1}{V(X)} \frac{\partial F(x)}{\partial \eta_{kl}} \Big|_{X,\eta'} = \frac{V(X)}{V(x)} a_{ik} a_{jl} \frac{1}{V(X)} \frac{\partial F(x)}{\partial \eta_{kl}} \Big|_{X,\eta'} \\ &= \frac{V(X)}{V(x)} a_{ik} a_{jl} \left[\tau_{kl}(X) + C(X)_{klmn} \eta_{mn} + \frac{1}{2} C(X)_{klmnpq} \eta_{mn} \eta_{pq} \right. \\ &\quad \left. + \frac{1}{6} C(X)_{klmnpqrs} \eta_{mn} \eta_{pq} \eta_{rs} + \dots \right],\end{aligned}\quad (\text{A1})$$

where $V(X) = V_0$ and $V(x) = V$ are the volume of the sample in undeformed state X and deformed state x . a_{ij} and $F(x)$ are the component of the deformation gradient matrix and the free energy. η_{ij} is the Lagrangian strain. Equation (A1) is obtained directly by using the relation between the Cauchy stress and the second Piola-Kirchhoff stress, which is $\sigma = J^{-1} a \tau a^T$, or more specifically $\sigma_{ij}(x) = \frac{V(X)}{V(x)} a_{ki} a_{lj} \tau_{kl}(x)$, where $\tau_{ij}(x) = \frac{1}{V(X)} \frac{\partial F(x)}{\partial \eta_{ij}} \Big|_{X,\eta'}$ is the Piola-Kirchhoff stress; $J = \det(a) = \frac{V(x)}{V(X)}$. The free energy F can be expressed as in the Taylor expansion in terms of the Lagrangian strain η ; the expression for F with up to fourth-order terms in η is

$$F(X, \eta, T) = F(X, 0, T) + V(X) \left[\tau_{ij}(X) \eta_{ij} + \frac{1}{2!} C_{ijkl}(X) \eta_{ij} \eta_{kl} + \frac{1}{3!} C_{ijklmn}(X) \eta_{ij} \eta_{kl} \eta_{mn} \right. \\ \left. + \frac{1}{4!} C_{ijklmnpq}(X) \eta_{ij} \eta_{kl} \eta_{mn} \eta_{pq} + \dots \right], \quad (\text{A2})$$

where $\tau_{ij}(X)$, C_{ijkl} , $C_{ijklmn}(X)$, and $C_{ijklmnpq}(X)$ are the second Piola-Kirchhoff stress and the second-, third-, and fourth-order elastic constants in the undeformed state. In this work, we use the experimentally measured elastic constants up to the fourth order in several bulk metallic glasses as inputs in the finite deformation theory (see Appendix E).

For pure shear deformation, the general strain tensor and deformation gradient matrix can be expressed as

$$\begin{pmatrix} \eta_{11} & \eta_{12} & 0 \\ \eta_{21} & \eta_{22} & 0 \\ 0 & 0 & \eta_{33} \end{pmatrix}$$

and

$$a = \begin{pmatrix} 1 + \eta_{11} - \frac{1}{2}(\eta_{11}^2 + \eta_{12}^2) & \eta_{12}(1 - \eta_{11}) & 0 \\ \eta_{12}(1 - \eta_{11}) & 1 + \eta_{11} - \frac{1}{2}(\eta_{11}^2 + \eta_{12}^2) & 0 \\ 0 & 0 & 1 + \eta_{33} - \frac{1}{2}\eta_{33}^2 \end{pmatrix},$$

respectively. The volume ratio equals to the determinant of the deformation gradient matrix, which is $\frac{V}{V_0} = \det(a)$. The normal strains in the relaxed case, η_{11} , η_{22} , and η_{33} , are induced by the shear deformation. Due to the symmetry in xy plane, we have $\eta_{11} = \eta_{22}$. By substituting the above-mentioned strain and the deformation gradient matrix into Eq. (A1), we can obtain the relation between the pure shear stress and strain which is expressed explicitly as

$$\begin{aligned}\sigma_{12} &= \frac{1}{V(x)} \frac{\partial F}{\partial \zeta_{12}} \Big|_x = \frac{V(X)}{V(x)} \sum_{kl} a_{1k} a_{2l} \left[\frac{1}{V(X)} \frac{\partial F}{\partial \eta_{kl}} \Big|_{X,\eta'} \right] \\ &= \frac{V(X)}{V(x)} \left\{ a_{11} a_{21} \left[\frac{1}{V(X)} \frac{\partial F}{\partial \eta_{11}} \Big|_{X,\eta'} \right] + a_{12} a_{22} \left[\frac{1}{V(X)} \frac{\partial F}{\partial \eta_{22}} \Big|_{X,\eta'} \right] \right. \\ &\quad \left. + a_{11} a_{22} \left[\frac{1}{V(X)} \frac{\partial F}{\partial \eta_{12}} \Big|_{X,\eta'} \right] + a_{12} a_{21} \left[\frac{1}{V(X)} \frac{\partial F}{\partial \eta_{21}} \Big|_{X,\eta'} \right] \right\},\end{aligned}\quad (\text{A3})$$

where 1, 2, and 3 are used to label the coordinate axes x , y , and z . The shear is on the x - y plane with the surface normal along the z direction.

With the same scheme, the components of the internal normal stresses in a pure shear sample can be obtained from Eq. (A1), which are

$$\sigma_{11} = \frac{1}{V} \frac{\partial F}{\partial \eta_{11}} \Big|_x = \frac{V_0}{V} \left[a_{11} a_{11} \left(\frac{1}{V_0} \frac{\partial F}{\partial \eta_{11}} \Big|_{X,\eta'} \right) + a_{12} a_{12} \left(\frac{1}{V_0} \frac{\partial F}{\partial \eta_{22}} \Big|_{X,\eta'} \right) + 2a_{11} a_{12} \left(\frac{1}{V_0} \frac{\partial F}{\partial \eta_{12}} \Big|_{X,\eta'} \right) \right], \quad (\text{A4a})$$

$$\sigma_{22} = \frac{1}{V} \frac{\partial F}{\partial \eta_{22}} \Big|_x = \frac{V_0}{V} \left[a_{21} a_{21} \left(\frac{1}{V_0} \frac{\partial F}{\partial \eta_{11}} \Big|_{X,\eta'} \right) + a_{22} a_{22} \left(\frac{1}{V_0} \frac{\partial F}{\partial \eta_{22}} \Big|_{X,\eta'} \right) + 2a_{21} a_{22} \left(\frac{1}{V_0} \frac{\partial F}{\partial \eta_{12}} \Big|_{X,\eta'} \right) \right] = \sigma_{11}, \quad (\text{A4b})$$

$$\sigma_{33} = \frac{1}{V} \frac{\partial F}{\partial \eta_{33}} \Big|_x = \frac{V_0}{V} \left(a_{33} a_{33} \frac{1}{V_0} \frac{\partial F}{\partial \eta_{33}} \Big|_{X,\eta'} \right). \quad (\text{A4c})$$

For metallic glasses under pure shear deformation, the strain derivatives of internal energy in the above expressions are

$$\begin{aligned} \frac{1}{V_0} \frac{\partial F}{\partial \eta_{11}} \Big|_{x, \eta'} &= C_{11} \eta_1 + C_{12} (\eta_2 + \eta_3) + \frac{1}{2} C_{111} \eta_1^2 + \frac{1}{2} C_{112} (2\eta_1^2 \eta_2 + 2\eta_1 \eta_3 + \eta_2^2 + \eta_3^2) \\ &\quad + C_{123} \eta_1 \eta_3 + \frac{1}{2} C_{155} \eta_6^2 + \frac{1}{6} C_{1111} \eta_1^3 + \frac{1}{6} C_{1112} (3\eta_1^2 (\eta_2 + \eta_3) + \eta_2^3 + \eta_3^3) \\ &\quad + \frac{1}{2} C_{1122} \eta_1 (\eta_2^2 + \eta_3^2) + \frac{1}{2} C_{1123} (2\eta_1 \eta_2 \eta_3 + \eta_2^2 \eta_3 + \eta_2 \eta_3^2) + \frac{1}{2} C_{1155} \eta_1 \eta_6^2 \\ &\quad + \frac{1}{2} C_{1255} \eta_3 \eta_6^2 + \frac{1}{2} C_{1266} \eta_2 \eta_6^2, \end{aligned} \quad (\text{A5a})$$

$$\frac{1}{V_0} \frac{\partial F}{\partial \eta_{22}} \Big|_{x, \eta'} = \frac{1}{V_0} \frac{\partial F}{\partial \eta_{11}} \Big|_{x, \eta'}, \quad (\text{A5b})$$

$$\begin{aligned} \frac{1}{V_0} \frac{\partial F}{\partial \eta_{33}} \Big|_{x, \eta'} &= C_{11} \eta_3 + C_{12} (\eta_1 + \eta_2) + \frac{1}{2} C_{111} \eta_3^2 + \frac{1}{2} C_{112} (\eta_1^2 + \eta_2^2) \\ &\quad + C_{112} (\eta_1 \eta_3 + \eta_2 \eta_3) + C_{123} \eta_1 \eta_2 + \frac{1}{2} C_{144} \eta_6^2 + \frac{1}{6} C_{1111} \eta_3^3 \\ &\quad + \frac{1}{6} C_{1112} (\eta_1^3 + \eta_2^3) + \frac{1}{2} C_{1112} \eta_3^2 (\eta_1 + \eta_2) + \frac{1}{2} C_{1122} \eta_3 (\eta_1^2 + \eta_2^2) \\ &\quad + \frac{1}{2} C_{1123} (\eta_1^2 \eta_2 + \eta_1 \eta_2^2 + 2\eta_1 \eta_2 \eta_3) + \frac{1}{2} C_{1144} \eta_3 \eta_6^2 + \frac{1}{2} C_{1255} (\eta_2 \eta_6^2 + \eta_1 \eta_6^2), \end{aligned} \quad (\text{A5c})$$

$$\begin{aligned} \frac{1}{V_0} \frac{\partial F}{\partial \eta_{12}} \Big|_{x, \eta'} &= C_{44} \eta_6 + C_{144} \eta_3 \eta_6 + C_{155} (\eta_1 + \eta_2) \eta_6 \\ &\quad + \frac{1}{2} C_{1144} \eta_3^2 \eta_6 + \frac{1}{2} C_{1155} (\eta_1^2 + \eta_2^2) \eta_6 + C_{1255} (\eta_1 \eta_3 + \eta_2 \eta_3) \eta_6 \\ &\quad + C_{1266} \eta_1 \eta_2 \eta_6 + \frac{1}{6} C_{4444} \eta_6^3, \end{aligned} \quad (\text{A5d})$$

where the Voigt notation is used for subscripts in the strains, such that 11 \rightarrow 1, 22 \rightarrow 2, 33 \rightarrow 3, 23 and 32 \rightarrow 4, 13 and 31 \rightarrow 5, and 21 and 12 \rightarrow 6.

Here we are going to use Eq. (A3) to study the pure shear deformation of metallic glasses. We will consider two different deformed states associated with the pure shear. One is the pure shear without relaxing out the normal stresses, i.e., $\sigma_{11} \neq 0$, $\sigma_{22} \neq 0$, and $\sigma_{33} \neq 0$, in which the normal strains are zero, i.e., $\eta_{11} = 0$, $\eta_{22} = 0$, and $\eta_{33} = 0$. We refer to this case as “unrelaxed.” As the values of normal strains in the unrelaxed sample are zero, the components of the shear-deformation-induced internal normal stress tensor can be expressed explicitly as

$$\sigma_1(x) = \sqrt{\frac{(1-2\eta_{12})}{(1+2\eta_{12})}} \left[-(C_{11} - C_{12}) \eta_{12} + \frac{1}{2} (C_{111} - C_{112}) \eta_{12}^2 + \frac{1}{6} (-C_{1111} + 4C_{1112} - 3C_{1122}) \eta_{12}^3 + \dots \right], \quad (\text{A6a})$$

$$\sigma_2(x) = \sqrt{\frac{(1+2\eta_{12})}{(1-2\eta_{12})}} \left[(C_{11} - C_{12}) \eta_{12} + \frac{1}{2} (C_{111} - C_{112}) \eta_{12}^2 + \frac{1}{6} (C_{1111} - 4C_{1112} + 3C_{1122}) \eta_{12}^3 + \dots \right], \quad (\text{A6b})$$

$$\sigma_3(x) = \frac{1}{\sqrt{(1+2\eta_{12})(1-2\eta_{12})}} [(C_{112} - C_{123}) \eta_{12}^2 + \dots]. \quad (\text{A6c})$$

The second is to relax out all the normal stresses, i.e., $\sigma_{11} = 0$, $\sigma_{22} = 0$, and $\sigma_{33} = 0$, and we refer to this case as “relaxed.” As a result of the normal stress relaxation, we have the induced normal strains, $\eta_{11} \neq 0$, $\eta_{22} \neq 0$, and $\eta_{33} \neq 0$. In Appendix B, we explain the procedure to get the normal strains and the shear stress in this case.

APPENDIX B

To obtain the shear stress-strain relation from Eq. (A1) or Eq. (A3) in the relaxed case, one first needs to get the shear-induced normal strains, η_{11} , η_{22} , and η_{33} , at each given applied shear strain η_{12} . This is done by solving Eqs. (A4a)–(A4c) where the shear-induced normal stresses σ_{11} , σ_{22} , and σ_{33} are set to zero. By solving these three auxiliary equations, (A4a)–(A4c), we obtain η_1 , η_2 , and η_3 , as well the volume ratio V/V_0 at each applied shear strain η_{12} .

Then we substitute the normal strains η_{11} , η_{22} , and η_{33} , the deformation gradient tensor a , and volume ratios $\frac{V_0}{V}$ back into Eq. (A3). With these quantities, we can proceed to obtain the shear stress by using Eq. (A3).

APPENDIX C

From the free energy in Eq. (A2), we can obtain the change of the elastic constants under pure shear deformation as follows [14]:

$$\begin{aligned}
C'_{ijkl}(x) &= \frac{1}{V(x)} \frac{\partial^2 F(x)}{\partial \zeta_{ij} \partial \zeta_{kl}} \Big|_x = \frac{V(X)}{V(x)} \frac{\partial \eta_{mm}}{\partial \zeta_{ij}} \frac{\partial \eta_{pq}}{\partial \zeta_{kl}} \frac{1}{V(X)} \frac{\partial^2 F(x)}{\partial \eta_{mm} \partial \eta_{pq}} \Big|_{X, \eta'} \\
&= \frac{V(X)}{V(x)} a_{im} a_{jn} a_{kp} a_{lq} \frac{1}{V(X)} \frac{\partial^2 F(x)}{\partial \eta_{mm} \partial \eta_{pq}} \Big|_{X, \eta'} \\
&= \frac{V(X)}{V(x)} a_{im} a_{jn} a_{kp} a_{lq} \left[C_{mnpq}(X) + c_{mnpquv}(X) \eta_{uv} \right. \\
&\quad \left. + \frac{1}{2} C_{mnpquvrs}(X) \eta_{uv} \eta_{rs} + \dots \right].
\end{aligned} \tag{C1a}$$

With the deformation gradient matrix a and the strain tensor, the nonzero components of the elastic constant matrix are

$$\begin{aligned}
C'_{11} = C'_{1111} &= \frac{V(X)}{V(x')} \sum_{kl} a_{1k} a_{1l} a_{1m} a_{1n} \left(\frac{1}{V(X)} \frac{\partial^2 F}{\partial \eta_{kl} \partial \eta_{mn}} \Big|_X \right) \\
&= \frac{V(X)}{V(x')} \left(\begin{aligned} &a_{11} a_{11} a_{11} a_{11} \frac{1}{V(X)} \frac{\partial^2 F}{\partial \eta_{11}^2} + 2 a_{11} a_{11} a_{12} a_{12} \frac{1}{V(X)} \frac{\partial^2 F}{\partial \eta_{11} \partial \eta_{22}} \\ &+ a_{12} a_{12} a_{12} a_{12} \frac{1}{V(X)} \frac{\partial^2 F}{\partial \eta_{22}^2} + 4 a_{11} a_{11} a_{11} a_{12} \frac{1}{V(X)} \frac{\partial^2 F}{\partial \eta_{12} \partial \eta_{11}} \\ &+ 4 a_{11} a_{12} a_{12} a_{12} \frac{1}{V(X)} \frac{\partial^2 F}{\partial \eta_{12} \partial \eta_{22}} + 4 a_{11} a_{12} a_{11} a_{12} \frac{1}{V(X)} \frac{\partial^2 F}{\partial \eta_{12}^2} \end{aligned} \right),
\end{aligned} \tag{C1b}$$

$$\begin{aligned}
C'_{22} = C'_{2222} &= \frac{V(X)}{V(x')} \sum_{kl} a_{2k} a_{2l} a_{2m} a_{2n} \left(\frac{1}{V(X)} \frac{\partial^2 F}{\partial \eta_{kl} \partial \eta_{mn}} \Big|_X \right) \\
&= \frac{V(X)}{V(x')} \left(\begin{aligned} &a_{21} a_{21} a_{21} a_{21} \frac{1}{V(X)} \frac{\partial^2 F}{\partial \eta_{11}^2} + 2 a_{21} a_{21} a_{22} a_{22} \frac{1}{V(X)} \frac{\partial^2 F}{\partial \eta_{11} \partial \eta_{22}} \\ &+ a_{22} a_{22} a_{22} a_{22} \frac{1}{V(X)} \frac{\partial^2 F}{\partial \eta_{22}^2} + 4 a_{21} a_{21} a_{21} a_{22} \frac{1}{V(X)} \frac{\partial^2 F}{\partial \eta_{12} \partial \eta_{11}} \\ &+ 4 a_{21} a_{22} a_{22} a_{22} \frac{1}{V(X)} \frac{\partial^2 F}{\partial \eta_{12} \partial \eta_{22}} + 4 a_{21} a_{22} a_{21} a_{22} \frac{1}{V(X)} \frac{\partial^2 F}{\partial \eta_{12}^2} \end{aligned} \right),
\end{aligned} \tag{C1c}$$

$$\begin{aligned}
C'_{33} = C'_{3333} &= \frac{V(X)}{V(x')} \sum_{kl} a_{3k} a_{3l} a_{3m} a_{3n} \left(\frac{1}{V(X)} \frac{\partial^2 F}{\partial \eta_{kl} \partial \eta_{mn}} \Big|_X \right) \\
&= \frac{V(X)}{V(x')} \left(a_{33} a_{33} a_{33} a_{33} \frac{1}{V(X)} \frac{\partial^2 F}{\partial \eta_{33}^2} \right),
\end{aligned} \tag{C1d}$$

$$\begin{aligned}
C'_{12} = C'_{1122} &= \frac{V(X)}{V(x')} \sum_{kl} a_{1k} a_{1l} a_{2m} a_{2n} \left(\frac{1}{V(X)} \frac{\partial^2 F}{\partial \eta_{kl} \partial \eta_{mn}} \Big|_X \right) \\
&= \frac{V(X)}{V(x')} \left(\begin{aligned} &a_{11} a_{11} a_{21} a_{21} \frac{1}{V(X)} \frac{\partial^2 F}{\partial \eta_{11}^2} + a_{11} a_{11} a_{22} a_{22} \frac{1}{V(X)} \frac{\partial^2 F}{\partial \eta_{11} \partial \eta_{22}} \\ &+ a_{12} a_{12} a_{22} a_{22} \frac{1}{V(X)} \frac{\partial^2 F}{\partial \eta_{22}^2} + a_{12} a_{12} a_{21} a_{21} \frac{1}{V(X)} \frac{\partial^2 F}{\partial \eta_{22} \partial \eta_{11}} \end{aligned} \right),
\end{aligned} \tag{C1e}$$

$$\begin{aligned}
C'_{13} = C'_{1133} &= \frac{V(X)}{V(x')} \sum_{kl} a_{1k} a_{1l} a_{3m} a_{3n} \left(\frac{1}{V(X)} \frac{\partial^2 F}{\partial \eta_{kl} \partial \eta_{mn}} \Big|_X \right) \\
&= \frac{V(X)}{V(x')} \left(\begin{aligned} &a_{11} a_{11} a_{33} a_{33} \frac{1}{V(X)} \frac{\partial^2 F}{\partial \eta_{33} \partial \eta_{11}} + a_{12} a_{12} a_{33} a_{33} \frac{1}{V(X)} \frac{\partial^2 F}{\partial \eta_{22} \partial \eta_{33}} \\ &+ 2 a_{11} a_{12} a_{33} a_{33} \frac{1}{V(X)} \frac{\partial^2 F}{\partial \eta_{33} \partial \eta_{12}} \end{aligned} \right),
\end{aligned} \tag{C1f}$$

$$\begin{aligned}
C'_{23} = C'_{2233} &= \frac{V(X)}{V(x')} \sum_{kl} a_{2k} a_{2l} a_{3m} a_{3n} \left(\frac{1}{V(X)} \frac{\partial^2 F}{\partial \eta_{kl} \partial \eta_{mn}} \Big|_X \right) \\
&= \frac{V(X)}{V(x')} \left(\begin{aligned} &a_{21} a_{21} a_{33} a_{33} \frac{1}{V(X)} \frac{\partial^2 F}{\partial \eta_{33} \partial \eta_{11}} + a_{22} a_{22} a_{33} a_{33} \frac{1}{V(X)} \frac{\partial^2 F}{\partial \eta_{33} \partial \eta_{22}} \\ &+ 2a_{21} a_{22} a_{33} a_{33} \frac{1}{V(X)} \frac{\partial^2 F}{\partial \eta_{33} \partial \eta_{12}} \end{aligned} \right), \tag{C1g}
\end{aligned}$$

$$\begin{aligned}
C'_{44} = C'_{2323} &= \frac{V(X)}{V(x')} \sum_{kl} a_{2k} a_{3l} a_{2m} a_{3n} \left(\frac{1}{V(X)} \frac{\partial^2 F}{\partial \eta_{kl} \partial \eta_{mn}} \Big|_X \right) \\
&= \frac{V(X)}{V(x')} \left(\begin{aligned} &a_{21} a_{33} a_{21} a_{33} \frac{1}{V(X)} \frac{\partial^2 F}{\partial \eta_{13}^2} + a_{22} a_{33} a_{22} a_{33} \frac{1}{V(X)} \frac{\partial^2 F}{\partial \eta_{23}^2} \\ &+ 2a_{21} a_{33} a_{22} a_{33} \frac{1}{V(X)} \frac{\partial^2 F}{\partial \eta_{13} \partial \eta_{23}} \end{aligned} \right), \tag{C1h}
\end{aligned}$$

$$\begin{aligned}
C'_{45} = C'_{1323} &= \frac{V(X)}{V(x')} \sum_{kl} a_{1k} a_{3l} a_{2m} a_{3n} \left(\frac{1}{V(X)} \frac{\partial^2 F}{\partial \eta_{kl} \partial \eta_{mn}} \Big|_X \right) \\
&= \frac{V(X)}{V(x')} \left(\begin{aligned} &a_{11} a_{33} a_{21} a_{33} \frac{1}{V(X)} \frac{\partial^2 F}{\partial \eta_{13}^2} + a_{12} a_{33} a_{22} a_{33} \frac{1}{V(X)} \frac{\partial^2 F}{\partial \eta_{23}^2} \\ &+ (a_{11} a_{33} a_{22} a_{33} + a_{12} a_{33} a_{21} a_{33}) \frac{1}{V(X)} \frac{\partial^2 F}{\partial \eta_{13} \partial \eta_{23}} \end{aligned} \right), \tag{C1i}
\end{aligned}$$

and

$$\begin{aligned}
C'_{66} = C'_{1212} &= \frac{V(X)}{V(x')} \sum_{kl} a_{1k} a_{2l} a_{1m} a_{2n} \left(\frac{1}{V(X)} \frac{\partial^2 F}{\partial \eta_{kl} \partial \eta_{mn}} \Big|_X \right) \\
&= \frac{V(X)}{V(x')} \left(\begin{aligned} &a_{11} a_{21} a_{11} a_{21} \frac{1}{V(X)} \frac{\partial^2 F}{\partial \eta_{11}^2} + 2a_{11} a_{21} a_{12} a_{22} \frac{1}{V(X)} \frac{\partial^2 F}{\partial \eta_{11} \partial \eta_{22}} \\ &+ a_{12} a_{22} a_{12} a_{22} \frac{1}{V(X)} \frac{\partial^2 F}{\partial \eta_{22}^2} + 2a_{11} a_{21} a_{11} a_{22} \frac{1}{V(X)} \frac{\partial^2 F}{\partial \eta_{12} \partial \eta_{11}} \\ &+ 2a_{11} a_{21} a_{12} a_{21} \frac{1}{V(X)} \frac{\partial^2 F}{\partial \eta_{21} \partial \eta_{11}} + 2a_{11} a_{22} a_{12} a_{22} \frac{1}{V(X)} \frac{\partial^2 F}{\partial \eta_{12} \partial \eta_{22}} \\ &+ 2a_{12} a_{21} a_{12} a_{22} \frac{1}{V(X)} \frac{\partial^2 F}{\partial \eta_{21} \partial \eta_{22}} + a_{11} a_{22} a_{11} a_{22} \frac{1}{V(X)} \frac{\partial^2 F}{\partial \eta_{12}^2} \\ &+ a_{12} a_{21} a_{12} a_{21} \frac{1}{V(X)} \frac{\partial^2 F}{\partial \eta_{21}^2} + 2a_{11} a_{22} a_{12} a_{21} \frac{1}{V(X)} \frac{\partial^2 F}{\partial \eta_{21} \partial \eta_{12}} \end{aligned} \right) \tag{C1j}
\end{aligned}$$

where the strain derivatives of the internal energy are

$$\begin{aligned}
\frac{1}{V(X)} \frac{\partial^2 F}{\partial \eta_{11}^2} \Big|_X &= C_{11} + C_{111} \eta_1 + C_{112} (\eta_2 + \eta_3) + \frac{1}{2} C_{1111} \eta_1^2 + C_{1112} \eta_1 (\eta_2 + \eta_3) \\
&\quad + \frac{1}{2} C_{1122} (\eta_2^2 + \eta_3^2) + C_{1123} \eta_2 \eta_3 + \frac{1}{2} C_{1155} \eta_6^2, \\
\frac{1}{V(X)} \frac{\partial^2 F}{\partial \eta_{22}^2} \Big|_X &= C_{11} + C_{111} \eta_2 + C_{112} (\eta_1 + \eta_3) + \frac{1}{2} C_{1111} \eta_2^2 + C_{1112} \eta_2 (\eta_1 + \eta_3) \\
&\quad + \frac{1}{2} C_{1122} (\eta_1^2 + \eta_3^2) + C_{1123} \eta_1 \eta_3 + \frac{1}{2} C_{1155} \eta_6^2, \\
\frac{1}{V(X)} \frac{\partial^2 F}{\partial \eta_{33}^2} \Big|_X &= C_{11} + C_{111} \eta_3 + C_{112} (\eta_1 + \eta_2) + \frac{1}{2} C_{1111} \eta_3^2 + C_{1112} \eta_3 (\eta_1 + \eta_2) \\
&\quad + \frac{1}{2} C_{1122} (\eta_1^2 + \eta_2^2) + C_{1123} \eta_1 \eta_2 + \frac{1}{2} C_{1144} \eta_6^2,
\end{aligned}$$

$$\begin{aligned}
\frac{1}{V(X)} \frac{\partial^2 F}{\partial \eta_{11} \partial \eta_{22}} \Big|_X &= C_{12} + C_{112}(\eta_1 + \eta_2) + C_{123}\eta_3 + \frac{1}{2}C_{1112}(\eta_1^2 + \eta_2^2) + C_{1122}\eta_1\eta_2 \\
&\quad + \frac{1}{2}C_{1123}(2\eta_1\eta_3 + 2\eta_2\eta_3 + \eta_3^2) + \frac{1}{2}C_{1266}\eta_6^2, \\
\frac{1}{V(X)} \frac{\partial^2 F}{\partial \eta_{11} \partial \eta_{33}} \Big|_X &= C_{12} + C_{112}(\eta_1 + \eta_3) + C_{123}\eta_2 + \frac{1}{2}C_{1112}(\eta_1^2 + \eta_3^2) + C_{1122}\eta_1\eta_3 \\
&\quad + \frac{1}{2}C_{1123}(2\eta_1\eta_2 + 2\eta_2\eta_3 + \eta_2^2) + \frac{1}{2}C_{1255}\eta_6^2, \\
\frac{1}{V(X)} \frac{\partial^2 F}{\partial \eta_{22} \partial \eta_{33}} \Big|_X &= C_{12} + C_{112}(\eta_2 + \eta_3) + C_{123}\eta_1 + \frac{1}{2}C_{1112}(\eta_1^2 + \eta_3^2) + C_{1122}\eta_1\eta_3 \\
&\quad + \frac{1}{2}C_{1123}(\eta_1^2 + 2\eta_1\eta_2 + 2\eta_1\eta_3) + \frac{1}{2}C_{1255}\eta_6^2, \\
\frac{1}{V(X)} \frac{\partial^2 F}{\partial \eta_{11} \partial \eta_{12}} \Big|_X &= \frac{1}{V(X)} \frac{\partial^2 F}{\partial \eta_{11} \partial \eta_6} \Big|_X = C_{155}\eta_6 + C_{1155}\eta_1\eta_6 + C_{1255}\eta_3\eta_6 + C_{1266}\eta_2\eta_6, \\
\frac{1}{V(X)} \frac{\partial^2 F}{\partial \eta_{22} \partial \eta_{12}} \Big|_X &= \frac{1}{V(X)} \frac{\partial^2 F}{\partial \eta_{22} \partial \eta_6} \Big|_X = C_{155}\eta_6 + C_{1155}\eta_2\eta_6 + C_{1255}\eta_3\eta_6 + C_{1266}\eta_1\eta_6, \\
\frac{1}{V(X)} \frac{\partial^2 F}{\partial \eta_{33} \partial \eta_{12}} \Big|_X &= \frac{1}{V(X)} \frac{\partial^2 F}{\partial \eta_{33} \partial \eta_6} \Big|_X = C_{144}\eta_6 + C_{1144}\eta_3\eta_6 + C_{1255}(\eta_2\eta_6 + \eta_1\eta_6), \\
\frac{1}{V(X)} \frac{\partial^2 F}{\partial \eta_{12}^2} \Big|_X &= \frac{1}{V(X)} \frac{\partial^2 F}{\partial \eta_6^2} \Big|_X = C_{44} + C_{144}\eta_3 + C_{155}(\eta_1 + \eta_2) + \frac{1}{2}C_{1144}\eta_3^2 + \frac{1}{2}C_{1155}(\eta_1^2 + \eta_2^2) \\
&\quad + C_{1255}(\eta_2\eta_3 + \eta_1\eta_3) + C_{1266}\eta_1\eta_2 + \frac{1}{2}C_{4444}\eta_6^2, \\
\frac{1}{V(X)} \frac{\partial^2 F}{\partial \eta_{13}^2} \Big|_X &= \frac{1}{V(X)} \frac{\partial^2 F}{\partial \eta_5^2} \Big|_X = C_{44} + C_{144}\eta_2 + C_{155}(\eta_1 + \eta_3) + \frac{1}{2}C_{1144}\eta_2^2 + \frac{1}{2}C_{1155}(\eta_1^2 + \eta_3^2) \\
&\quad + C_{1255}(\eta_1\eta_2 + \eta_2\eta_3) + C_{1266}\eta_1\eta_3 + \frac{1}{2}C_{4455}\eta_6^2, \\
\frac{1}{V(X)} \frac{\partial^2 F}{\partial \eta_{23}^2} \Big|_X &= \frac{1}{V(X)} \frac{\partial^2 F}{\partial \eta_4^2} \Big|_X = C_{44} + C_{144}\eta_1 + C_{155}(\eta_2 + \eta_3) + \frac{1}{2}C_{1144}\eta_1^2 + \frac{1}{2}C_{1155}(\eta_2^2 + \eta_3^2) \\
&\quad + C_{1255}(\eta_1\eta_2 + \eta_1\eta_3) + C_{1266}\eta_2\eta_3 + \frac{1}{2}C_{4455}\eta_6^2,
\end{aligned}$$

and

$$\frac{1}{V(X)} \frac{\partial^2 F}{\partial \eta_{13} \partial \eta_{23}} \Big|_X = \frac{1}{V(X)} \frac{\partial^2 F}{\partial \eta_5 \partial \eta_6} \Big|_X = 0,$$

where C and C' are the elastic constants in the undeformed and deformed state, respectively. For the unrelaxed sample, the only nonzero strain is η_6 . While after the induced normal stresses are relaxed out (see Appendix B), the nonzero normal strains are η_1 , η_2 , η_3 , and η_6 . For the given values of the shear and normal strains, we can obtain the elastic constant components by Eqs. (C1a)–(C1j).

APPENDIX D

From the stresses in Eq. (A3), Eqs. (A6), and the elastic constants in Eqs. (C1a)–(C1j), we have the components of the elastic stiffness constant matrix from the definition $\hat{B}_{ij} = \frac{1}{2}(B_{ij} + B_{ij}^T)$, where $B_{ijkl} = C'_{ijkl} + (\delta_{ik}\tau_{jl} + \delta_{jk}\tau_{il} + \delta_{il}\tau_{jk} + \delta_{jl}\tau_{ik} - 2\delta_{kl}\tau_{ij})/2$.

Here, the components of the elastic stiffness matrix under pure shear loading are

$$\begin{aligned}
\bar{B}_{11} &= \bar{B}_{22} = C'_{11} + \sigma_{11}, \\
\bar{B}_{12} &= C'_{12} - \sigma_{11}, \\
\bar{B}_{13} &= \bar{B}_{23} = C'_{13} - (\sigma_{11} + \sigma_{33})/2, \\
\bar{B}_{33} &= C'_{33} + \sigma_{33}, \\
\bar{B}_{44} &= \bar{B}_{55} = C'_{44} + (\sigma_{11} + \sigma_{33})/2, \\
\bar{B}_{45} &= C'_{45} + \sigma_{12}/2, \\
\bar{B}_{66} &= C'_{66} + \sigma_{11}, \\
\bar{B}_{16} &= \bar{B}_{26} = C'_{16} + \sigma_{12}/2, \\
\bar{B}_{36} &= C'_{36} - \sigma_{12}/2, \\
&\text{and} \\
\bar{B}_{ij} &= 0, \text{ all others.}
\end{aligned} \tag{D1}$$

For the case with the induced normal stress relaxed out, the normal stresses will be zero, i.e., $\sigma_{11} = 0$, $\sigma_{22} = 0$, and $\sigma_{33} = 0$. The stability criterion $|\bar{B}| \rightarrow 0$ leads to the following six conditions:

$$\bar{B}_{11} > 0, \tag{D2a}$$

$$\bar{B}_{11}^2 - \bar{B}_{12}^2 > 0, \tag{D2b}$$

$$(\bar{B}_{11} + \bar{B}_{12})\bar{B}_{33} - 2\bar{B}_{13}^2 > 0, \tag{D2c}$$

$$\bar{B}_{44} > 0, \tag{D2d}$$

$$\bar{B}_{44}^2 - \bar{B}_{45}^2 > 0, \tag{D2e}$$

and

$$(\bar{B}_{11} + \bar{B}_{12})(\bar{B}_{33}\bar{B}_{66} - \bar{B}_{36}^2) - 2\bar{B}_{16}(\bar{B}_{16}\bar{B}_{33} - \bar{B}_{13}\bar{B}_{36}) - 2\bar{B}_{13}(\bar{B}_{13}\bar{B}_{66} - \bar{B}_{16}\bar{B}_{36}) > 0. \tag{D2f}$$

By using the elastic stable criteria [(D2a)–(D2f)], we can obtain the elasticity stability conditions of the deformed sample under the pure shear deformation.

APPENDIX E

In the finite deformation theoretical formulation, stresses and elastic constants are a function of the elastic constants in the undeformed state and the applied shear strain. Using the input of second-, third-, and fourth-elastic constants measured in the samples, we can obtain both the shear stress-strain and the elastic constants in any deformed state via Eqs. (A3) and (C1), as well as the stability criterion via Eq. (D2). The input elastic constants are shown in Table II.

-
- | | |
|---|---|
| [1] J. Frenkel, <i>Z. Phys.</i> 37 , 572 (1926). | [16] H. Wang and M. Li, <i>J. Phys.: Condens. Matter.</i> 24 , 245402 (2012). |
| [2] P. B. Hirsch, R. W. Home, and M. J. Whelan, <i>Philos. Mag.</i> 1 , 677 (1956). | [17] J. Wang, S. Yip, S. R. Phillpot, and D. Wolf, <i>Phys. Rev. Lett.</i> 71 , 4182 (1993). |
| [3] J. R. Greer, <i>Rev. Adv. Mater. Sci.</i> 13 , 59 (2006). | [18] N. P. Kobelev, E. L. Kolyvanov, and V. A. Khonik, <i>Phys. Solid State</i> 49 , 1209 (2007). |
| [4] T. Zhu and J. Li, <i>Prog. Mater. Sci.</i> 55 , 710 (2010). | [19] N. P. Kobelev, E. L. Kolyvanov, and V. A. Khonik, <i>Phys. Solid State</i> 57 , 1483 (2015). |
| [5] H. Wang and M. Li, <i>Phys. Rev. B</i> 85 , 104103 (2012). | [20] R. J. Wang, F. Y. Li, Z. C. Qin, and W. H. Wang, <i>Chin. Phys. Lett.</i> 18 , 414 (2001). |
| [6] A. T. Paxton, P. Gumbsch, and M. Methfessel, <i>Philos. Mag. Lett.</i> 63 , 267 (1991). | [21] M. Luckabauer, U. Kühn, J. Eckert, and W. Sprengel, <i>Phys. Rev. B</i> 89 , 174113 (2014). |
| [7] J. Pokluda, M. Černý, P. Šandera, and M. Šob, <i>J. Comput.-Aided Mater. Des.</i> 11 , 1 (2004). | [22] S. C. Glade, R. Busch, D. S. Lee, W. L. Johnson, R. K. Wunderlich, and H. J. Fecht, <i>J. Appl. Phys.</i> 87 , 7242 (2000). |
| [8] S. Ogata, Y. Umeno, and M. Kohyama, <i>Modell. Simul. Mater. Sci. Eng.</i> 17 , 013001 (2009). | [23] S. Chantasiriwan and F. Milstein, <i>Phys. Rev. B</i> 58 , 5996 (1998). |
| [9] H. Wang and M. Li, <i>J. Phys.: Condens. Matter.</i> 22 , 295405 (2010). | [24] P. S. Branício and J.-P. Rino, <i>Phys. Rev. B</i> 62 , 16950 (2000). |
| [10] S. S. Brenner, <i>J. Appl. Phys.</i> 27 , 1484 (1956). | [25] H. Bei, Z. P. Lu, and E. P. George, <i>Phys. Rev. Lett.</i> 93 , 125504 (2004). |
| [11] M. L. Jokl, V. Vitek, and C. J. McMahon, Jr., <i>Acta Metall.</i> 28 , 1479 (1980). | [26] H. Bei, Z. P. Lu, S. Shim, G. Chen, and E. P. George, <i>Metall. Mater. Trans. A</i> 41 , 1735 (2010). |
| [12] R. Thomson, <i>Solid State Phys.</i> 39 , 1 (1986). | |
| [13] Y. Luo, Q. K. Li, and M. Li, <i>J. Appl. Phys.</i> 117 , 044301 (2015). | |
| [14] Z. K. Zhou, H. Wang, and M. Li (unpublished). | |
| [15] D. C. Wallace, <i>Thermodynamics of Crystals</i> (Dover, New York, 1998). | |

- [27] R. T. Qu, J. Eckert, and Z. F. Zhang, *J. Appl. Phys.* **109**, 869 (2011).
- [28] C. Chen, M. Gao, C. Wang, W. H. Wang, and T. C. Wang, *Sci. Rep.* **6**, 39522 (2016).
- [29] G. K. Liao, Z. L. Long, M. S. Z. Zhao, L. Peng, W. Chai, and Z. H. Ping, *Phys. B (Amsterdam, Neth.)* **534**, 163 (2018).
- [30] I. Hussain, Y. Y. Jiang, Y. D. Jia, G. Wang, Q. J. Zhai, K. C. Chan, and J. Yi, *Sci. Rep.* **8**, 5659 (2018).
- [31] J. Lu, G. Ravichandran, and W. L. Johnson, *Acta Mater.* **51**, 3429 (2003).
- [32] M. F. Ashby and A. L. Greer, *Scr. Mater.* **54**, 321 (2006).
- [33] H. Wang and M. Li, *Phys. Rev. Lett.* **111**, 065507 (2013).
- [34] J. P. Hirth and J. Lothe, *Theory of Dislocations* (Wiley, New York, 1982).
- [35] M. Polanyi, *Z. Phys.* **7**, 323 (1921).
- [36] E. Orowan, *Rep. Prog. Phys.* **12**, 185 (1949).
- [37] G. I. Taylor, *Trans. Faraday Soc.* **24**, 121 (1928).
- [38] R. E. Peierls, *Proc. Phys. Soc., London* **52**, 34 (1940).
- [39] F. R. N. Nabarro, *Theory of Crystal Dislocations* (Dover Publications, New York, 1987), original publication (Clarendon Press, Oxford, 1967).
- [40] D. Hull and D. J. Bacon, *Introduction to Dislocations*, 5th ed. (Butterworth-Heinemann, Oxford, 2011).
- [41] G. P. Zheng and M. Li, *Phys. Rev. B* **80**, 104201 (2009).